Detection of HCl molecules by resonantly enhanced sum-frequency mixing of mid- and near-infrared laser pulses

Benedikt Moneke,* Jan Frederic Kinder, Oskar Ernst, and Thomas Halfmann
Institut für Angewandte Physik, Technische Universität Darmstadt, Hochschulstrasse 6, 64289 Darmstadt, Germany

(Received 10 October 2022; accepted 19 December 2022; published 5 January 2023)

We perform experimental studies of resonantly enhanced sum-frequency mixing (SFM), driven by tunable, spectrally narrowband mid-infrared and fixed-frequency nanosecond laser pulses, aiming at applications in molecular gas detection. The mid-infrared pulses are tuned in the vicinity of two-photon rovibrational transitions in the electronic ground state to provide strong resonance enhancements of the nonlinear susceptibility, while a probe laser at shorter wavelength uses an off-resonant single-photon coupling to excited electronic states. This SFM approach benefits from the advantageous combination of typically small detunings among the mid-infrared, vibrational transitions and the typically large transition dipole moment for couplings of electronic states. Moreover, compared to resonantly enhanced third harmonic generation (THG), a signal wave at much shorter wavelength permits simple and efficient detection. We demonstrate resonantly enhanced SFM via rovibrational states in gaseous hydrogen chloride molecules and compare its features to THG. The SFM spectra offer a large signal-to-noise ratio of 4 orders of magnitude and a detection limit down to a pressure of 0.1 mbar, corresponding to a particle density of 0.35×10^{15} per cm^3.

DOI: 10.1103/PhysRevA.107.012803

I. INTRODUCTION

Nonlinear laser spectroscopy offers a multitude of techniques for sensitive detection of molecular species, as required for trace gas analysis, environmental sensing, combustion diagnostics, or microscopy [1–4]. Approaches based on four-wave mixing (FWM) are a prominent class of such techniques, with the ability to isolate the generated signals spectrally and spatially from the driving laser fields [5]. The probably most established FWM technique for spectroscopy is coherent anti-Stokes Raman scattering (CARS) [6,7]. Figure 1(a) schematically depicts the coupling scheme, in which a pump and a Stokes field with frequencies ω_p and ω_st generate an anti-Stokes field at the CARS signal frequency $\omega_\mathrm{s} = 2\omega_\mathrm{p} - \omega_\mathrm{st}$ in the molecular species. When the laser frequencies $\omega_\mathrm{p} - \omega_\mathrm{st}$ are tuned to a two-photon vibrational resonance between the ground state $|0\rangle$ and an excited state $|1\rangle$, mediated via off-resonant coupling to higher states $|e\rangle$, the signal yield is strongly enhanced. For CARS, the pump and Stokes usually operate in the visible or near-ultraviolet regime [5]. The large single-photon transition dipole moment to electronically excited states $|e\rangle$ reaches typical values of several 10^{-30} Cm. The anti-Stokes signal wave is typically in the visible or near-infrared regime, which is easily accessible by sensitive photodetectors. However, CARS requires two laser fields. Moreover, while we tune the lasers in CARS to a two-photon resonance (two-photon detuning $\delta_2 = 0$), the one- and three-photon detunings δ_1 and δ_3 to the excited electronic states $|e\rangle$ are usually still very large with several 10 000 cm^{-1} [see Fig. 1(a)]. This limits the obtained nonlinear susceptibility and signal yield.

Resonantly enhanced third harmonic generation [THG, see Fig. 1(b)] is a simpler approach, as it involves only a single driving field. The fundamental field at fundamental frequency ω_f generates the third harmonic at $\omega_\mathrm{s} = 3\omega_\mathrm{f}$. When we drive THG with mid-infrared laser pulses in the vicinity of rovibrational levels in the electronic ground state of a molecule, we can tune the laser frequency to either single-, two-, or three-photon resonance and achieve resonance enhancement of the THG process. At single-photon resonance the molecules would absorb a significant portion of the fundamental radiation. Hence, mid-infrared THG usually operates at two- or three-photon resonance. Let us consider a two-photon resonance, as depicted at the transition $|0\rangle \rightarrow |2\rangle$ in Fig. 1(b). An important feature of mid-infrared THG in the vicinity of rovibrational molecular states is that at two-photon resonance $\delta_2 = 0$ also the one- and three-photon detunings δ_1 and δ_3 at the dominating transitions to neighbor vibrational states remain small, typically in the range of 10–100 cm^{-1} only. This is due to the small anharmonicity of low-lying vibrational states. The simultaneously small detunings $\delta_{1,2,3}$ substantially enhance the nonlinear susceptibility for mid-infrared THG [8]. This is another advantage compared to CARS. However, the rovibrational transition moments are usually smaller compared to electronic transition moments relevant for CARS, reaching typically only values $\leqslant 10^{-30}$ Cm. This holds in particular for the overtone transition moment between the highest involved rovibrational state $|3\rangle$ and the ground state $|0\rangle$ in mid-infrared THG with $\Delta v = 3$ [see Fig. 1(b)], which is typically only 0.001×10^{-30} Cm. Thus, mid-infrared THG benefits from small detunings, but also suffers from small transition moments compared to CARS. Moreover, the generated signal for mid-infrared THG is typically still in the infrared spectral range, which is only accessible with less sensitive detectors.

*Benedikt.Moneke@physik.tu-darmstadt.de

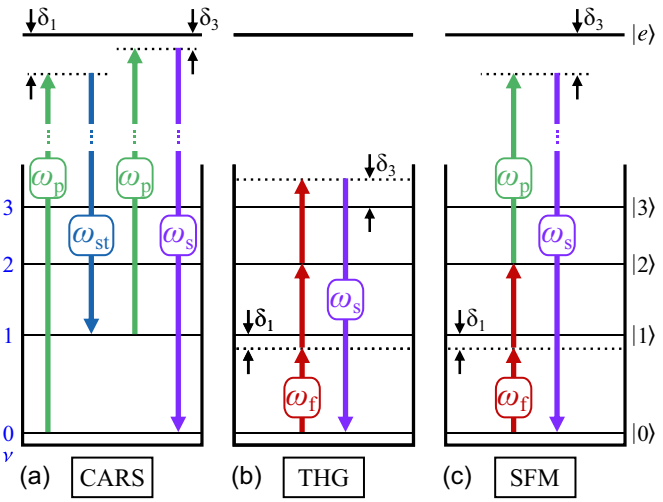

FIG. 1. Coupling schemes for (a) CARS, (b) THG, and (c) SFM. For simplicity, we show only the vibrational states $|v\rangle$ of the electronic ground state, but not their rotational substructure, nor details of the excited electronic state(s) $|e\rangle$. Arrows indicate laser fields at the fundamental (ω_f, red), probe (ω_p, green, in the case of CARS also called "pump"), Stokes (ω_{st}, blue), and generated signal (ω_s, purple) frequency while δ_i indicates the i-photon detuning. We assume the lasers are tuned to two-photon resonance with vibrational states in the electronic ground state.

There is another approach to nonlinear FWM spectroscopy, which can combine the benefits of CARS and THG [9]. Resonantly enhanced sum-frequency mixing (SFM) applies a fundamental mid-infrared field at ω_f, tuned to a two-photon rovibrational resonance [see transition $|0\rangle \rightarrow |2\rangle$ in Fig. 1(c)], and a visible or near-infrared probe field at ω_p to generate a signal at the sum frequency $\omega_s = 2\omega_f + \omega_p$. Similar to THG, also at two-photon resonance $\delta_2 = 0$, the single-photon detuning δ_1 remains small with typically a few 10 cm^{-1}. For the probe field, couplings to higher electronic states $|e\rangle$ dominate. Hence, the three-photon detuning δ_3 is rather large (typically a few 10 000 cm^{-1}, as in CARS), but we also benefit from the large electronic transition moment as in CARS, e.g., on the transition between the electronically excited states $|e\rangle$ and the ground state $|0\rangle$. The nonlinear susceptibilities for all the discussed FWM processes, CARS, THG, and SFM, depend upon the ratio of transition moments and detunings. As we see below, the discussed combination of transition moments and detunings in SFM is the most advantageous for the nonlinear susceptibility. This permits SFM involving a mid-infrared two-photon transition to outperform THG and CARS. Moreover, the obtained SFM signal is typically in the visible or near-infrared regime, which allows for sensitive and efficient detection, as in CARS. Also similar to CARS, probe pulses at fixed frequency are often available from the laser setup "for free" and at large pulse energy, e.g., as residual radiation from a strong pump laser. This further boosts the signal yield, e.g., compared to THG driven by tunable mid-infrared laser pulses with typically rather limited pulse energy. Finally, noncollinear beam geometries permit spatial separation of the signal wave from the fundamental and probe waves, which improves the signal-to-noise ratio.

The basic idea of resonantly enhanced SFM was already proposed decades ago for spectroscopy in infrared-active molecules [9]. However, due to the lack of continuously tunable, narrowband, and sufficiently intense mid-infrared laser sources, there were no further studies nor a convincing experimental demonstration. There was only a review of the initial proposal [10] and a recent experiment which applied a related approach to enhance the nonlinear susceptibility of Raman scattering via a two-photon vibrational resonance in methane [7]. However, the latter work operated at huge particle pressure of up to several atmospheres (far beyond realistic applications in trace detection), did not provide data to demonstrate better performance of SFM compared to THG or CARS, and applied broadband picosecond pulses. The latter are spectrally too broad to take full advantage of resonance enhancements or to permit spectral resolution of rotational transitions (which is required, e.g., for temperature determination). For an experimental demonstration we require mid-infrared laser pulses with narrow spectral bandwidth and large pulse energy. Hence, intense laser pulses with nanosecond (ns) duration and a Fourier transform-limited bandwidth in the range of 0.01 cm^{-1} are an appropriate choice. The bandwidth is in the same range as a typical Doppler-broadened linewidth of a rovibrational transition at room temperature [11]. In the following we present a convincing experimental demonstration of resonantly enhanced SFM via mid-infrared rovibrational transitions in a molecular gas. Towards this goal we apply a compact, home-made laser system based on an optical parametric oscillator and amplifiers to provide tunable, mid-infrared (ns) laser pulses with bandwidth close to the Fourier transform limit and pulse energies in the mJ regime. We compare SFM with resonantly enhanced THG, in particular, with regard to its applicability for sensitive molecule detection.

II. BASICS OF RESONANTLY ENHANCED SUM-FREQUENCY MIXING

Consider FWM of a mid-infrared fundamental field at ω_f and a visible or infrared probe field at ω_p to generate a signal at $\omega_s = 2\omega_f + \omega_p$ in a molecular gas [see Fig. 1(c)]. The fundamental laser is tuned to two-photon resonance with the transition between the rovibrational ground state $|0\rangle$ and an excited state $|2\rangle$, while it is detuned from all single-photon transitions. The probe laser couples, typically quite off-resonant, state $|2\rangle$ in the electronic ground state to a manifold of excited electronic states $|e\rangle$, respectively the vibrational states therein. For simplicity, we assume the transition to a single, excited vibronic state $|e\rangle$. Without the probe field, the fundamental radiation alone drives THG to yield a signal at $3\omega_f$. The power P of the generated SFM signal for focused Gaussian beams is [12]

$$P(\omega_s;\,\omega_f,\omega_p) = \frac{\omega_s\,\omega_f^2\,\omega_p}{4\pi^2\epsilon_0^2 c^6}\; b^{-2}|\chi^{(3)}|^2\;|J_3(\Delta k)|^2\;P_f^2\;P_p, \quad (1)$$

with the power of the incoming waves P_f and P_p, the third-order dielectric susceptibility $\chi^{(3)}$, and the confocal parameter b. We assume negligible absorption of all involved waves, which is well justified for operation sufficiently far from vibrational and electronic single-photon resonances. $J_3(\Delta k)$ is

the phase-matching integral [12],

$$J_3(\Delta k) = \int_{z_0}^{z_1} \frac{e^{i\,\Delta k\, z} dz}{(1 + 2iz/b)^2}, \tag{2}$$

for collinearly propagating Gaussian beams, with focus $z = 0$, interaction region between z_0 and z_1, and the wave vector mismatch $\Delta k = 2k_\mathrm{f} + k_\mathrm{p} - k_\mathrm{s}$ involving the wave vectors $k_i = n_i\omega_i/c$ with the refractive indices n_i.

In Eq. (1), the nonlinear dielectric susceptibility contains the relevant spectroscopic information of the molecular medium [12]

$$\chi^{(3)}(\omega_\mathrm{s}; \omega_\mathrm{f}, \omega_\mathrm{p}) = \frac{1}{\epsilon_0 \hbar^3} \sum_k \frac{\rho\, \mu_{10}\, \mu_{21}\, \mu_{e2}\, \mu_{e0}}{(\delta_1 - i\gamma_1)(\delta_2 - i\gamma_2)(\delta_3 - i\gamma_3)}, \tag{3}$$

with the number density ρ of molecules in the ground state $|0\rangle$, the single-photon detuning $\delta_1 = \omega_{01} - \omega_\mathrm{f}$, the two-photon detuning $\delta_2 = \omega_{02} - 2\omega_\mathrm{f}$, the three-photon detuning $\delta_3 = \omega_{0e} - 2\omega_\mathrm{f} - \omega_\mathrm{p}$, involving transition frequencies ω_{ij} between states $|i\rangle$ and $|j\rangle$, the corresponding transition dipole moments μ_{ij}, and the dephasing rates (linewidth) γ_i. In general, we have to sum over all possible k multiphoton excitation pathways in the molecule to generate the signal wave, also involving the manifold of detuned, excited rovibronic states. For simplicity, we ignore the summation in the following discussion, as it does not affect our basic arguments. Typically, specific pathways dominate this sum, when one or several of the detunings δ_i for the specific pathway are much smaller (at or near resonance) than for others. In this case, the specific single-, two-, or three-photon resonant pathway gives the largest contribution to the nonlinear susceptibility and generated signal power (compare Fig. 1). This permits species-selective molecule detection by "fingerprint" spectra.

With Eq. (3) we very roughly estimate the third-order nonlinear susceptibility of two-photon ($\delta_2 = 0$) resonantly enhanced CARS, THG, and SFM in a small molecule. We assume typical values for the vibrational transition dipole moments with 1×10^{-30} Cm, except for the third overtone with 0.001×10^{-30} Cm, electronic transition dipole moments of 3×10^{-30} Cm, detunings to the vibrational states of 30 cm^{-1}, detuning to the excited electronic state 30 000 cm^{-1}, pressure of 1 mbar (we assume all molecules to be in state $|0\rangle$) and Doppler broadened linewidth of 200 MHz [full width at half maximum (FWHM)]. Pressure broadening is negligible at such low pressure. With these values, the absolute value of $\chi^{(3)}$ is 10 $\mathrm{pm}^2/\mathrm{V}^2$ for CARS, 100 $\mathrm{pm}^2/\mathrm{V}^2$ for THG, and 1000 $\mathrm{pm}^2/\mathrm{V}^2$ for SFM. This indicates the advantage of SFM compared to THG and CARS. Exact values for the nonlinear susceptibility will vary with the specific molecule, as the dipole moments enter Eq. (3) in a fourfold product and detunings in a threefold product. In general, we must also consider a contribution of the excited electronic states to the THG yield—which we neglected here to simplify the introductory discussion. Nevertheless, the advantages of SFM remain under typical conditions for molecular species.

III. EXPERIMENTAL SETUP

We performed the experiments in hydrogen chloride (HCl) molecules as a test gas. HCl is a relevant product from combustion processes, especially of biomass [13] or polyvinyl chloride compounds [14]. Due to the toxic and corrosive nature, detection of HCl is highly desirable even at low concentrations. We use gas samples (supplied by Westfalen) with a purity of 99.5% and a residual moisture of <50 ppm. HCl has two stable isotopes, with natural abundances of 76% in H ^{37}Cl and 24% in H ^{37}Cl [11]. The transitions between the low-vibrational states are at a wavelength of 3.5 μm. The first excited electronic state has an energy of roughly 63 700 cm^{-1} [15]. For a probe laser at 1064 nm, the detuning δ_3 to this excited electronic state is 48 600 cm^{-1}. However, as discussed above, the typically large electronic transition dipole moments μ_{e2} and μ_{e0} more than compensate for the large detuning. We note that transitions between the vibrational levels in the electronic ground state driven by the probe laser play no role, as the probe couples states with $\Delta\nu \gg 1$ (i.e., high overtone transitions) with negligible transition probability. For the same reason, reabsorption of the THG and SFM signal radiation is negligible. This is a typical situation for most molecules and a probe laser in the visible or near-infrared regime.

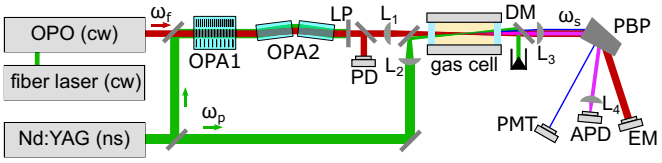

FIG. 2. Experimental setup with (cw) fiber pump laser, (cw) optical parametric oscillator (OPO), pre-amplifier (OPA1), power amplifier (OPA2), Nd:YAG pump laser, longpass filter (LP), lenses (L), photodiode (PD), dichroic mirror (DM), Pellin-Broca prism (PBP), photomultiplier tube (PMT), avalanche photodiode (APD), and energy meter (EM). Note the angle between the beams in the gas cell to indicate a noncollinear geometry.

The laser setup (see Fig. 2) involves a continuous-wave (cw) optical parametric oscillator (OPO), with a preamplifier and amplifier (optical parametric amplifier), emitting 6-ns (FWHM)-long pulses at 3.2−3.9 μm with more than 1 mJ. The two amplification steps convolute the temporal pump profile with itself, resulting in a shorter pulse duration. The center wavelength λ_f of the (ns) pulses follows the wavelength tuning of the (cw) OPO, which is implemented by tuning the wavelength of the fiber pump laser. An injection-seeded Nd:YAG laser (Pro 230, Spectra Physics) generates (ns) pulses at a wavelength of $\lambda_\mathrm{p} = 1064$ nm, a pulse energy of 1.3 J, and a duration of 8 ns (FWHM) at a repetition rate of 20 Hz to pump the OPA stages and provide the probe pulses for the SFM process. For details on the laser system, see Refs. [8,16]. The pulses from the OPO/OPA system serve as mid-infrared fundamental radiation to drive THG and SFM in HCl. A wavemeter (WS6-600, High Finesse) measures the frequency of the fiber laser in the (cw) OPO to indirectly monitor the fundamental frequency. We determine the absolute fundamental wavelength by absorption spectroscopy in HCl. An InAsSb photo detector (P13243-011MA, Hamamatsu Photonics), calibrated with an energy meter (PE-10C, Ophir), monitors the pulse energy of the mid-infrared fundamental radiation. The beam is mildly focused by an antireflection-coated CaF_2 lens (L_1) with a focal length of 250 mm into a gas cell (length

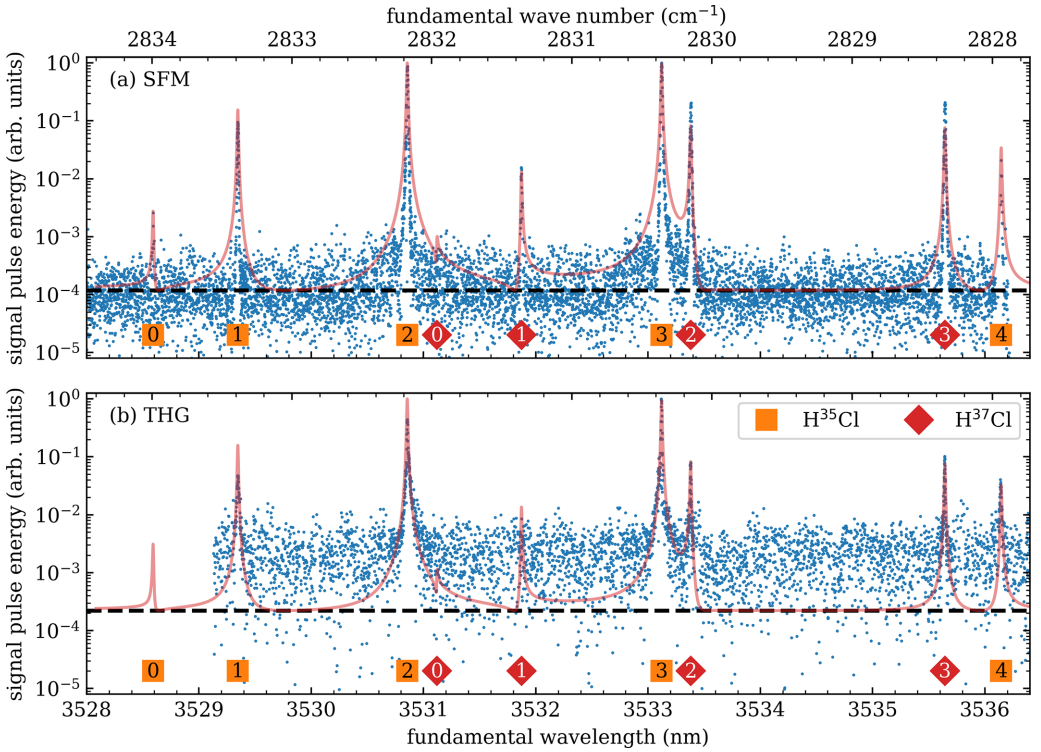

FIG. 3. (a) SFM and (b) THG signal pulse energy vs fundamental wavelength (or wave number on the upper axis). The signal pulse energy is normalized to the maximum value in each data set. The fundamental peak intensity was 360 MW/cm^2 (pulse energy 1.2 mJ) for SFM and 300 MW/cm^2 (pulse energy 1 mJ) for THG. The probe peak intensity was 2.9 GW/cm^2 (pulse energy 1.2 mJ). Blue dots indicate experimental data, averaged in wavelength bins of 1 pm. The red line shows a numerical simulation with the mean background (dashed black line) as offset. For simplicity and faster calculation, we assumed a Lorentzian line shape instead of a Voigt profile. Markers indicate the central wavelengths of rovibrational two-photon resonances ($v = 0 \rightarrow 2$, Q-branch with $\Delta N = 0$ in the electronic ground state), with rotational quantum numbers N of the ground state for the transition (orange squares for H ^{35}Cl, red diamonds for H ^{37}Cl). Note that the logarithmic scale on the pulse-energy axes limits the presentation of the background to positive values, though it contains negative values due to electronic noise as well.

18 cm) with uncoated, wedged CaF_2 windows, which contains the HCl gas. We monitor the pressure with a combination of a piezo sensor and a Pirani sensor (VCR, Thyracont), which we calibrate for HCl.

The focus of the mid-infrared fundamental beam in the gas cell has an extension of 183 μm ($1/e^2$ radius) and the confocal parameter is 60 mm. At a typical pulse energy of 1 mJ, the peak intensity of the fundamental beam in the gas cell is 300 MW/cm^2. The probe beam is focused by a lens system (L_2) consisting of two uncoated CaF_2 lenses (focal lengths of 200 and 250 mm) into the gas cell, yielding a focal spot with an extension of 55 μm ($1/e^2$ radius) and a confocal parameter of 18 mm. The peak intensity of the probe beam reaches 2.4 GW/cm^2 at a typical pulse energy of 1 mJ. Fundamental and probe beams have equal, linear polarization. The fundamental pulse has a delay of 1 ns with respect to the probe pulse at the place of the gas cell. To reduce the optical background (which was due to SFM in the window cells), in most measurements we applied a slightly noncollinear beam geometry with a small angle of 1° between the fundamental and the probe beam.

Prior to detection, we separate the SFM signal at a wavelength of 660 nm or the THG signal at a wavelength of 1.2 μm from the intense probe beam with a dichroic mirror (DM, coated for high reflectivity at 1064 nm and high transmission at mid-infrared wavelengths, Laseroptik). A CaF_2 lens (L_3) with a focal length of 250 mm collimates the signal beams and a CaF_2 Pellin-Broca prism further separates the signals from residual probe and fundamental radiation. The SFM signal passes a bandpass filter (FB650-40, Thorlabs) and is detected by a photomultiplier tube (PMT, R4220, Hamamatsu). The THG signal pulses pass two spectral edgepass filters (FELH1100, Thorlabs; No. 89-675, Edmund Optics) to remove stray light, and an AR coated lens L_4 focuses the signal onto the active area (200 μm in diameter) of an InGaAs avalanche photodiode (APD, IAG200S6, Laser Components), equipped with an amplifier (DLPCA-200, Femto). We calibrated the PMT and APD with attenuated laser pulses at 532 nm [second harmonic of the (ns) Nd:YAG pump laser] and 1064 nm, respectively. Calibrated neutral density filters in front of the THG and SFM detectors attenuate the signal pulse energy as required. This serves to relate the detector signal S to the number of photons N_c in the calibration pulses. We adjust the photon number at signal wavelength N_s to the detector quantum efficiencies η_c and η_s at the calibration and signal wavelengths via the relation $N_s(S) = N_c(S)\,\eta_c/\eta_s$.

IV. EXPERIMENTAL RESULTS

Figures 3(a) and 3(b) show SFM and THG spectra in HCl at a pressure of 29 mbar, while tuning the fundamental mid-infrared wavelength in the vicinity of rovibrational two-

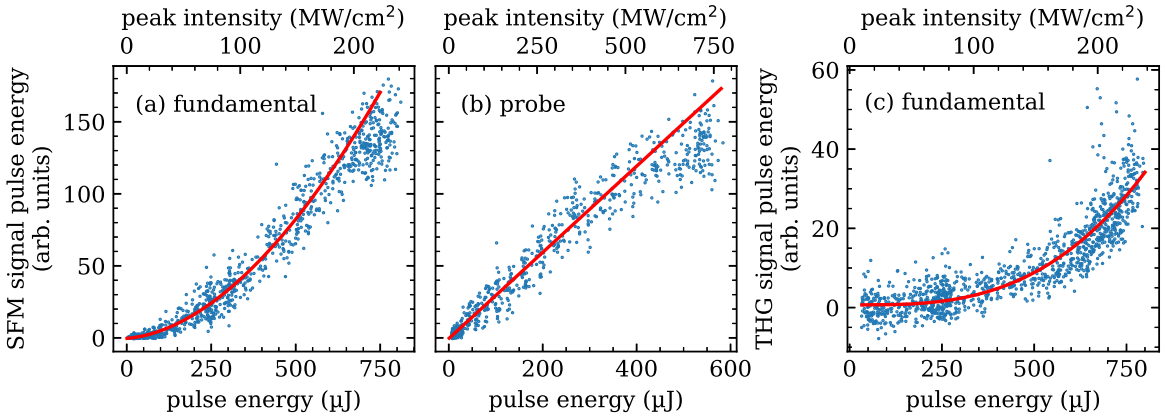

FIG. 4. SFM signal pulse energy vs (a) fundamental and (b) probe pulse energy (or peak intensity on the upper axis). The pulse energy of the other beam was kept at 500 μJ. Collinear beam geometry (probe beam waist of 175 μm). (c) THG signal pulse energy vs fundamental pulse energy. The HCl pressure was 57 mbar for all measurements. Blue points show experimental data. The red line shows an exponential fit.

photon resonances of the two isotopes. We kept the probe pulse intensity at a comparable level to the fundamental pulse intensity in order to permit a "fair" comparison of the SFM and THG spectra. However, much more probe pulse energy would be available from the Nd:YAG laser to further boost the SFM yield. The experimental data fit well with the numerical simulation. Note that the logarithmic scale of the signal axes in Fig. 3 exaggerates some small deviation in the low-intensity wings of the experimentally determined SFM line profile compared to the simulation. The background is mainly due to electronic noise of the detection setup. Obviously, the noise level in the SFM spectrum is much lower, despite a comparable mean value of the background signal. The larger noise amplitude does not permit observation of the resonance expected at 3531.87 nm (ground state $N = 1$ in $H^{37}Cl$) in the THG spectrum, while the latter resonance is clearly visible in the SFM spectrum. When we compare the weak spectral line at a fundamental wavelength of 3528.59 nm (ground state $N = 0$ in $H^{35}Cl$) with the strong resonance at 3533.12 nm (ground state $N = 3$ in $H^{35}Cl$), we find a ratio of 1/400 for their line intensities. Therefore, we expect from Eq. (3) to still obtain signal above the noise level down to pressures below 1.5 mbar at the strong resonance. This already indicates the potential of this approach for detection at low pressures, which we will discuss in more detail below. Furthermore, the signal-to-noise ratio, i.e., SFM signal level compared to the standard deviation of the background, reaches almost 4 orders of magnitude at the strong resonance. We verified that there is only THG signal and no SFM signal at three-fundamental-photon resonances (outside the depicted wavelength tuning range), as expected for the rather short probe laser wavelength towards a visible SFM signal.

To confirm the expected mixing processes, we consider the intensity dependence of the SFM signal. We measured the variation of the SFM signal pulse energy vs fundamental and probe pulse energy [Figs. 4(a) and 4(b)] at the strongest resonance of $H^{35}Cl$ at a fundamental wavelength of 3533.12 nm (ground state $N = 3$). Exponential fits to the experimental data yield a power dependence with an exponent of 1.9(2) for the fundamental field [compared to an expected value of 2, see Eq. (1)] and 0.9(1) for the probe field (compared to an expected value of 1). This confirms that the detected signal is indeed due to SFM. For comparison, Fig. 4(c) shows the THG signal pulse energy as it varies with the fundamental pulse energy. An exponential fit to the experimental data yields an exponent of 2.9(6), which is close to the expected value of 3. In the center of the beam, we calculate the peak pulse area (product of two-photon Rabi frequency Ω and pulse duration τ) as $\Omega\tau \approx 8$. Averaging over the beam profile, we get an average pulse area well below unity. Thus, there are no saturation effects yet, as confirmed by our data. We assume that saturation of the PMT causes the SFM signal pulse energy to deviate from the exponential fit above a value of 120 arbitrary units.

We discuss the pressure dependence of the SFM signal. In particular, we determine the detection limit, which is the most important feature for a potential application of SFM spectroscopy. For maximal signal yield, we tuned the fundamental wavelength to the strongest two-photon resonance of $H^{35}Cl$ with $N(v = 0) = 3$ ($\lambda_f = 3533.12$ nm) and operated the laser system at a fundamental and probe pulse energy of 1.1 mJ. For comparison, we performed the same measurement for THG with a fundamental pulse energy of 1 mJ.

Figure 5(a) shows the number of SFM signal photons per pulse when we varied the HCl pressure. We performed two sets of measurements, either by a continuous variation of the pressure at fixed fundamental wavelength tuned to the expected two-photon resonance (see blue solid line in the figure), as well as by recording full spectral line profiles [see Fig. 5(c)] at the transition for selected pressures. We fit Voigt profiles to the latter experimental data and indicate the maxima of the fitted profiles with orange symbols in Fig. 5(a). This made sure that we observed the signal yield exactly at the resonance position, even if the latter varied slightly due to pressure-induced line shifts. We noticed a line shift up to 0.03 cm^{-1} at atmospheric pressure. Thus, pressure-induced resonance shifts play no role in the low-pressure range relevant for applications—as already a quick comparison of the two measurement sets in Fig. 5(a) shows.

The pressure dependence yields an exponential growth for a signal level exceeding background noise. The exponent of 1.7(1) for SFM is very close to the predicted exponent of

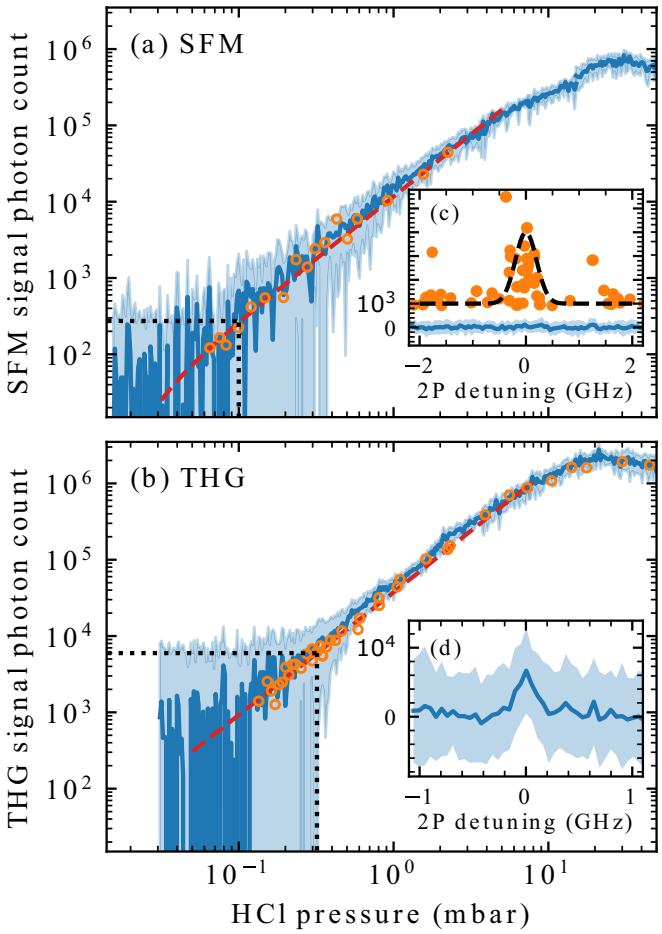

FIG. 5. (a) SFM and (b) THG signal photon count per pulse vs HCl pressure. The blue line represents experimental data from continuous variation of the HCl pressure at fixed fundamental wavelength (3533.12 nm), binned in 0.01 logarithmic decade pressure intervals. The blue shaded area indicates the standard deviation. Orange hollow circles show the maxima of Voigt fits to spectral lines at selected pressures. The red dashed line is an exponential fit to the latter data. Black dotted lines mark the noise level and detection limit. Note the logarithmic scales on both axes. The insets show the spectral lines [photon count per pulse vs two-photon (2P) detuning] at the detection limit, for (c) SFM at 0.1 mbar and for (d) THG at 0.32 mbar. For SFM, we distinguish between the electronic background in blue and the optical signal as orange dots. The black dashed line is added to guide the eye.

1.9 from our numerical simulation. We note that from simple theory (neglecting phase-matching issues), we would expect an exponent of 2 for any nonlinear optical frequency conversion process. This is due to the nonlinear susceptibility, which grows linearly with the number density ρ, which is proportional to the HCl pressure. Hence, the signal intensity grows with the square of the pressure [compare Eq. (1)]. However, phase matching changes this behavior, because at larger pressure phase mismatch reduces the signal yield [see phase-matching integral in Eq. (2)]. As a consequence, the signal yield grows with a slightly lower exponent than 2 for low pressures, reaches a maximum in an intermediate regime, and decreases for large pressures. We confirmed this behavior in SFM measurements towards larger pressures up to 700 mbar. From the data we obtain a maximal SFM signal at a pressure around 30 mbar, while the signal decreases due to phase-matching issues at larger pressures. Our numerical simulation confirms these findings. Buffer gas might affect the phase-matching integral. The situation is slightly different in THG spectroscopy [see in Fig. 5(b)], where we observe an exponent of 1.6(1), while the simulation yields 2.3. However, this prediction depends a lot upon exact numbers for refractive indices, which are not known with sufficient precision.

From the data in Fig. 5 we determine a detection limit for THG and SFM, i.e., the minimal particle pressure which still permits observation of a spectral line. More accurately, we define the detection limit by the HCl pressure, at which the mean signal pulse energy exceeds the standard deviation of the background [see Figs. 5(a) and 5(b)]. For SFM, the detection limit is 0.1 mbar (corresponding to 0.35×10^{15} H ^{35}Cl particles per cm^3 in the relevant ground state). As expected, this is well below 1.5 mbar, which we roughly estimated as an upper limit from the SFM spectrum. For THG, the detection limit is around 0.32 mbar (corresponding to 1.2×10^{15} particles per cm^3), which is an improvement compared to our previous work on resonantly enhanced THG [8]. Nevertheless SFM outperforms THG with regard to the detection limit. Even below the detection pressure limit defined by the above condition, we can identify spectral lines (see orange data points below the detection limits in Fig. 5), albeit with less confidence.

Figures 5(c) and 5(d) show spectral lines at the detection limit for SFM and THG. For THG, the peak appears on top of large electronic noise, which is due to the need for amplification of the APD signal. This is a major and typical disadvantage of THG signal detection by an APD compared to the SFM scheme with a PMT. Also in the SFM measurement we find a constant baseline of electronic noise (see blue line) adding to optically generated signal (see orange dots), which also contains optical background due to scattered radiation in the setup and ambient light. Nevertheless, the SFM peak at the detection limit is clearly visible. The electronic noise in SFM detection could be further reduced, if we apply a PMT with larger efficiency. The PMT in our setup had a still rather low quantum efficiency of only a few percent. There are devices with larger quantum efficiency in the relevant spectral range, which would further boost SFM detection.

Finally we briefly discuss the signal photon yield and conversion efficiency in our THG and SFM experiments. From basic theory (see above), we would expect a larger signal photon number and conversion efficiency in SFM. A simplified estimation of the nonlinear susceptibility $\chi^{(3)}$ at an HCl pressure of 30 mbar (of which 14% are in the relevant isotope and ground state) yields values of 117 pm^2/V^2 for THG and 145 pm^2/V^2 for SFM. The estimation also includes the electronic contribution to the THG yield via the far-off-resonant coupling of state $|2\rangle$ to the electronically excited state(s) $|e\rangle$, which is also driven by the mid-infared wave. This contribution is not negligible compared to the coupling via the vibrational state $|3\rangle$ in HCl. The values for the susceptibilities are lower than our rough estimation due to small transition dipole moments in HCl. By estimations we confirmed that many other molecules with relevance for applications, e.g.,

CO_2, have substantially larger nonlinear susceptibilities. The phase-matching integral in the calculation for SFM assumes ideal conditions of perfectly collinear geometry and equal confocal parameters for fundamental and probe beams. Extension of the treatment for noncollinear Gaussian beams and different confocal parameters will be part of future work. An angle between the beams increases the phase mismatch, which reduces the phase-matching integral, as well as the effective interaction length [17]. Therefore, we expect a lower signal for noncollinear (or nonperfect) SFM. The experimental data confirm this expectation: The photon count and the conversion efficiency for THG are somewhat larger than in SFM [compare signals for large pressures in Figs. 5(a) and 5(b)]. From the data we roughly estimate the absolute value of the nonlinear susceptibility $\chi^{(3)}$ for THG as 25 $\mathrm{pm}^2/\mathrm{V}^2$. If we take the uncertainty in our calibration of the detection setup for absolute photon numbers into account, this roughly fits to the range of the theoretically expected value. From the SFM data we would get a value of 20 $\mathrm{pm}^2/\mathrm{V}^2$ if we assumed a collinear configuration (which is not the case). This lower than expected value probably mirrors the effect of the phase-matching integral, as discussed above. Nevertheless, even in this case the nonlinear susceptibility for SFM compensates for the losses due to the phase-matching integral and shorter effective interaction length, which in turn reduces the background noise efficiently. Thus, the obtained signal-to-noise ratio is far better in SFM compared to THG. Even under the not optimal conditions for SFM, we achieved a lower detection limit compared to THG. There are several options for further improvements, e.g., using a probe at shorter wavelength (i.e., smaller detuning to the electronically excited states, which permits even larger nonlinear susceptibility), applying a PMT better suited for the SFM signal wavelength, increasing the probe pulse energy, or applying SFM in setups without cell windows (as it is the case, e.g., for combustion diagnostics), which produced perturbing optical background in our experiments.

V. CONCLUSION

We performed experimental studies on resonantly enhanced SFM of spectrally narrow, mid-infrared (ns) fundamental laser pulses and intense, fixed-frequency, near-infrared (ns) probe pulses for molecule detection. The SFM approach benefits from a large resonance enhancement of the nonlinear susceptibility on a rovibrational two-photon transition at small detunings of the involved couplings. This is similar to resonantly enhanced THG in the mid-infrared regime. Moreover, SFM benefits from the larger transition moment to excited electronic states driven by a probe laser at shorter wavelength. This is similar to CARS. Moreover, SFM yields a signal at shorter (typically visible) wavelength, which permits simple and efficient detection compared to signals from resonantly enhanced THG at long wavelength.

In our experiments, we used HCl molecules in a cell as a test gas. We provide the fundamental mid-infrared (ns) pulses by a homemade laser system, which delivers (ns) pulses, broadly tunable between 3.2 and 3.9 μm, with a spectral bandwidth of 108 MHz (FWHM) close to the Fourier transform limit, and pulse-energies beyond 1 mJ. The probe laser pulses are provided by a Nd:YAG laser at 1064 nm.

We recorded SFM and THG spectra when we tuned the mid-infrared fundamental laser pulses across rovibrational transitions in the electronic ground state of HCl. SFM clearly outperforms THG, reaching a signal-to-noise ratio of 4 orders of magnitude in "molecular fingerprint" spectra. The dependence of the process upon the driving laser pulse energies confirms the expected behavior of SFM, i.e., quadratic on the fundamental pulse energy and linear with the probe pulse energy. We also determined the dependence of the SFM signal pulse energy with particle pressure, yielding an exponential growth of the signal with an exponent of 1.7, which fits with the calculated value of 1.9 for small pressures below 10 mbar (close to quadratic dependence if we ignore phase-matching effects). From the pressure data we determine the detection limits of SFM and THG in our setup: SFM allows detection of a signal well resolvable from the electronic and optical background down to a HCl pressure of 0.1 mbar, which corresponds to a particle density of 0.35×10^{15} per cm^3. In comparison, we confidently detected a THG signal down to 0.32 mbar HCl pressure. A background gas would increase the linewidth and therefore the detection limit for both (or any other) techniques. Even much lower detection limits for SFM are in reach by straightforward technical improvements of the setup. The experimental data, confirmed by numerical simulations, demonstrate the potential of the SFM approach to detect molecular gases.

ACKNOWLEDGMENTS

We acknowledge experimental assistance by F. Wanitschke and L. Meyer, as well as support with the numerical simulations by N. Stewen and by P. Christ. This work was funded by the Deutsche Forschungsgemeinschaft (DFG, German Research Foundation) under Grant No. 290467699.

APPENDIX: PARAMETERS FOR THE NUMERICAL SIMULATION

The simulation applies Eq. (1) to calculate the SFM signal pulse energy in gaseous HCl, involving the phase-matching integral according to Eq. (2) and the third-order nonlinear susceptibility $\chi^{(3)}$ from Eq. (3). For THG, we set the probe frequency and power equal to the fundamental frequency and power. The calculation requires state energies, transition wavelengths, rovibrational transition dipole moments, and line broadenings (natural, collisional, and Doppler broadening) as parameters for the relevant rovibrational states and transitions in the electronic ground state of HCl. These values are available from the HITRAN data base [11]. The HITRAN database does not provide data for electronic transitions. Due to the large detuning from the excited electronic states, it is justified to approximate the manifold of rovibronic transitions by a single transition between the states $A(^1\Pi) \leftarrow X(^l\Sigma^+)$. We calculate three-photon detunings and transition dipole moments from parameters given in Ref. [15]. The relevant detunings to the excited electronic state are $\delta_3(\mathrm{THG}) = 55\,228\ \mathrm{cm}^{-1}$ for THG and $\delta_3(\mathrm{SFM}) = 48\,661\ \mathrm{cm}^{-1}$ for SFM. From spectroscopic data [15] we estimate electronic transition

dipole moments in the range of $\mu_{e2} \approx \mu_{e0} = 3 \times 10^{-30}$ Cm for both THG and SFM.

For the line shape we assume (for simplicity) a Lorentzian line profile with a linewidth (half width at half maximum) determined from a Voigt profile involving the dephasing rate γ of the optical transitions in Eq. (3), taking natural linewidth, collisional broadening, and Doppler broadening for the fundamental wavelength into account [18]. We restrict the calculation to vibrational states $\nu \leqslant 3$ in the sum over multiphoton excitation pathways k. This is well justified, as the detunings to higher vibrational states increase and the transition moments quickly decrease. Moreover, in the sum we consider only transitions obeying the selection rules $\Delta\nu = \pm 1$ and $\Delta N = \pm 1$. To calculate the phase-matching integral we require the refractive indices for all involved waves. Following Refs. [19,20], we obtain the refractive index n of HCl for a frequency ω at a given temperature T and pressure p as

$$n(\omega, T, p) = \sqrt{1 + \chi^{(1)}(\omega, T, p)} + \frac{p\,(n_0 - 1)}{p_{\mathrm{ref}}\,(1 + \alpha T)}, \quad \text{(A1)}$$

with a temperature coefficient of $\alpha = 3.66 \times 10^{-3}\,^{\circ}\mathrm{C}^{-1}$ for HCl [20] and a reference pressure of $p_{\mathrm{ref}} = 1013$ mbar. n_0 is a refractive index offset taken from Ref. [20] for the signal wavelengths and taken from Ref. [19] for the fundamental wavelength. We calculate the linear susceptibility $\chi^{(1)}$ according to Ref. [12] for all possible transitions in the $\nu = 0 \rightarrow 1$ and $\nu = 0 \rightarrow 3$ absorption band. The required parameters are also taken from the HITRAN database.

[1] R. L. Farrow and D. J. Rakestraw, Science **257**, 1894 (1992).
[2] V. Ebert, C. Schulz, H.-R. Volpp, J. Wolfrum, and P. Monkhouse, Isr. J. Chem. **39**, 1 (1999).
[3] M. R. Leahy-Hoppa, J. Miragliotta, R. Osiander, J. Burnett, Y. Dikmelik, C. McEnnis, and J. B. Spicer, Sensors **10**, 4342 (2010).
[4] J.-X. Cheng and X. S. Xie, J. Phys. Chem. B **108**, 827 (2004).
[5] J. Kiefer and P. Ewart, Prog. Energy Combust. Sci. **37**, 525 (2011).
[6] S. A. Druet and J. P. E. Taran, Prog. Quantum Electron. **7**, 1 (1981).
[7] A. J. Traverso, B. Hokr, Z. Yi, L. Yuan, S. Yamaguchi, M. O. Scully, and V. V. Yakovlev, Phys. Rev. Lett. **120**, 063602 (2018).
[8] J. F. Kinder, F. Cipura, and T. Halfmann, Phys. Rev. A **103**, 052808 (2021).
[9] M. J. Pellin and J. T. Yardley, Appl. Phys. Lett. **29**, 304 (1976).
[10] A. A. Makarov and E. A. Ryabov, Usp. Fiz. Nauk **189**, 271 (2019).
[11] I. Gordon, L. Rothman, C. Hill, R. Kochanov, Y. Tan, P. Bernath, M. Birk, V. Boudon, A. Campargue, K. Chance, B. Drouin, J.-M. Flaud, R. Gamache, J. Hodges, D. Jacquemart, V. Perevalov, A. Perrin, K. Shine, M.-A. Smith, J. Tennyson *et al.* J. Quant. Spectrosc. Radiat. Transfer **203**, 3 (2017).
[12] R. W. Boyd, *Nonlinear Optics*, 4th ed. (Academic, London, 2020).
[13] X. Ren, R. Sun, H. H. Chi, X. Meng, Y. Li, and Y. A. Levendis, Fuel **200**, 37 (2017).
[14] A. A. Stec, T. R. Hull, K. Lebek, J. A. Purser, and D. A. Purser, Fire Mater. **32**, 49 (2008).
[15] G. F. Adams and C. F. Chabalowski, J. Phys. Chem. **98**, 5878 (1994).
[16] J. F. Kinder, B. Moneke, O. Ernst, and T. Halfmann, Appl. Phys. B **128**, 188 (2022).
[17] G. C. Bjorklund, IEEE J. Quantum Electron. **11**, 287 (1975).
[18] J. Olivero and R. Longbothum, J. Quant. Spectrosc. Radiat. Transfer **17**, 233 (1977).
[19] J. E. Chamberlain, F. D. Findlay, and H. A. Gebbie, Appl. Opt. **4**, 1382 (1965).
[20] R. Rollefson and A. H. Rollefson, Phys. Rev. **48**, 779 (1935).